PAPER • OPEN ACCESS

Strong light–matter coupling in microcavities characterised by Rabi-splittings comparable to the Bragg stop-band widths

To cite this article: Junhui Cao *et al* 2021 *New J. Phys.* **23** 113015

New Journal of Physics
The open access journal at the forefront of physics

Deutsche Physikalische Gesellschaft DPG
IOP Institute of Physics

Published in partnership with: Deutsche Physikalische Gesellschaft and the Institute of Physics

OPEN ACCESS

RECEIVED
19 July 2021

REVISED
10 October 2021

ACCEPTED FOR PUBLICATION
22 October 2021

PUBLISHED
9 November 2021

PAPER

Strong light–matter coupling in microcavities characterised by Rabi-splittings comparable to the Bragg stop-band widths

Junhui Cao[1,2], **Simone De Liberato**[3] **and Alexey V Kavokin**[1,2,*]

[1] Westlake University, 18 Shilongshan Road, Hangzhou 310024, Zhejiang Province, People's Republic of China
[2] Institute of Natural Sciences, Westlake Institute for Advanced Study, 18 Shilongshan Road, Hangzhou 310024, Zhejiang Province, People's Republic of China
[3] School of Physics and Astronomy, University of Southampton, Southampton, SO17 1BJ, United Kingdom
[*] Author to whom any correspondence should be addressed.

E-mail: a.kavokin@westlake.edu.cn

Keywords: optical Rabi splitting, organic microcavity, strong light–matter coupling

Abstract

The vacuum Rabi splitting of polaritonic eigenmodes in semiconductor microcavities scales with the square root of the oscillator strength, as predicted by the coupled oscillator model and confirmed in many experiments. We show here that the square root law is no more applicable if the Rabi splitting becomes comparable or larger than the stop-band width of the Bragg mirrors forming the cavity. Once the oscillator strength becomes large enough, the material hosting excitons hybridises with the quasi-continuum microcavity Bragg modes lying outside of the stop-band, thus forming a novel kind of polaritonic resonance. We study this physics considering both two- and three-dimensional excitonic materials embedded in the microcavity. We highlight the varied phenomenology of those polaritons and develop a theoretical understanding of their most peculiar features.

1. Introduction

Quantum wells (QWs) embedded in semiconductor Bragg microcavities have been one of the first systems in which the resonant mode splitting between light and matter has been observed [1]. The study of exciton–polaritons, the hybrid light–matter excitations of such heterostructures, have blossomed in an extremely rich field of research, with proposed applications spanning optoelectronics [2], superconductivity [3], analog simulations [4], quantum technologies [5], optical computing [6], and machine learning [7].

Most studies to date have focused on an idealised system in which a single excitonic resonance couples to a single discrete photonic mode. Such an approach is adequate when the coupling between light and matter is larger than the intrinsic resonance linewidth, but otherwise much smaller than all the other energy scales. It instead breaks down when, exploiting a number of advances in the design of both resonators and quantum emitters [8], the coupling becomes comparable to other energy scales, ushering us into a zoology of non-perturbative coupling regimes [9, 10].

In particular, when the coupling becomes comparable to the energy difference between different matter resonances [11], the interaction between light and matter doesn't cause only Rabi oscillations between the bare light and matter excitations, but it can modify the electronic wavefunction of the system [12]. In this way polaritonics becomes a tool to modify the underlying electronic properties of the material [13]. The impact of such physics becomes even greater when the effect of the ionization continuum is taken into account, causing not only renormalization of the system's parameters [14, 15], but also the possibility of creating novel bound excitons kept together by photon exchange [16, 17].

In this work we investigate the dual case in which the interaction energy between a discrete excitonic resonance and a microcavity exceeds the width of the microcavity stopband, thus coupling to the complex quasi-continuum structure of Bragg-modes. To this aim we consider two model systems, schematised in figure 1. In figure 1(a), a thin layer of dipoles is placed at the center of a microcavity. For definiteness we

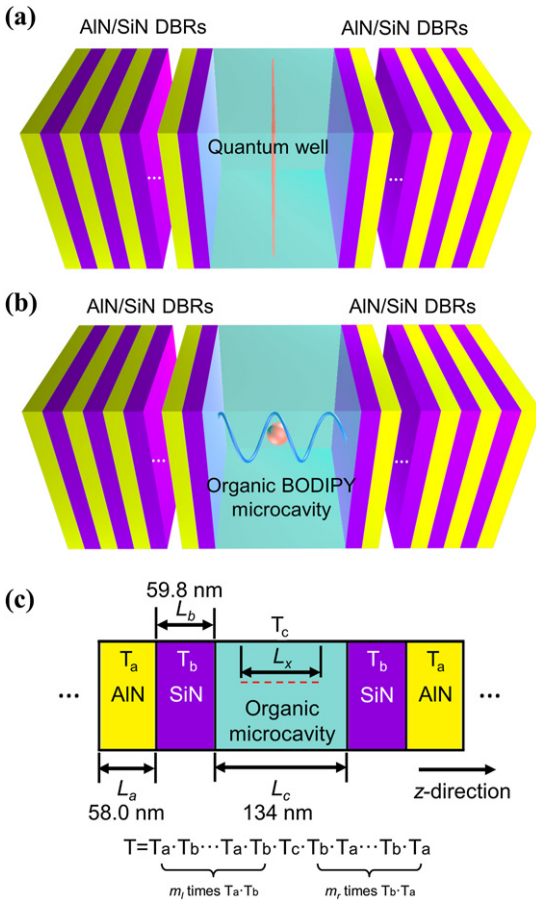

Figure 1. Schematic illustration of the two classes of planar optical microcavities considered in this work. (a) The central layer between the two mirrors is filled with an optically inert material embedding a thin excitonic material in its center, e.g. a QW. (b) The central layer between the two mirrors is filled with a bulk excitonic material, e.g. organic molecules with large oscillator strength like BODIPY. (c) Parameters of elementary cells in the structure. T_a, T_b and T_c in equation (7) stand for the transfer matrices of AlN, SiN mirror and microcavity, with length of L_a, L_b and L_c, respectively. L_x indicates the length of excitonic material in microcavity. The transfer matrix T across the entire structure is multiplication of elementary transfer matrix of optical layers. The expression shown is for the case $L_x = L_c$ in which the cavity is completely filled with excitonic material. m_l and m_r indicate the number of optical unit cells composing left and right Bragg mirror.

will refer to this layer as a QWs [18, 19], but it could as well describe other two-dimensional materials embedded in the microcavity [20–22]. In figure 1(b) instead the cavity is completely filled by a bulk homogeneous excitonic material, as organic molecules [23] or polar dielectrics hosting bulk optical phonons.

In a rigorous semiclassical framework we consider the vacuum Rabi frequency, quantifying the light–matter coupling strength, as an adjustable parameter, varying from zero to the frequency of the bare optical transition. Note that although achievable couplings in inorganic excitonic microcavities are substantially smaller [8], interesting effects become apparent already for values of the coupling comparable with the microcavity stopband width. Such a regime can be achieved by combining microcavities with narrow index contrast with samples with multiple QWs [12], or 2D material layers [24]. Organic microcavities are instead characterised by much larger light–matter coupling strengths when compared to their inorganic counterparts [25, 26], allowing to cover much of the parameter space considered in this paper. Moreover, the coupling strength of organic microcavities can be optically modified [27], allowing us to tune the distributed Bragg reflector (DBR) reflectivity *in situ*.

We start by presenting the transfer matrix semiclassical calculation of the model microcavity response which will allow us to predict a number of effects in different configurations, namely: (i) the deviation of the Rabi-splitting dependence on the exciton oscillator strength from the well-known square root law, (ii) the strong coupling of exciton with both the cavity photon mode and some of the Fabry–Pérot modes confined between upper and lower surfaces of the structure (Bragg modes), (iii) a parity filtering effect that consists in the coexistence of the strong coupling regime of the exciton with Bragg modes of a certain parity and zero exciton-coupling with modes of the opposite parity, (vi) a strongly asymmetric reflectivity, due to the opening of a polaritonic Reststrahlen band. We will also verify that some of the features we observe can

be reproduced with a simplified quasimode quantum approach, thus strengthening the relevance of our modal interpretation.

2. Theoretical framework

2.1. Model systems

We consider a model structure that represents an optical microcavity sandwiched between two identical Bragg mirrors, as shown in figure 1, each mirror being a finite-size DBR. Each DBR represents a periodic structure whose period is composed of two different layers with thicknesses L_a and L_b and refractive indices n_a and n_b. The Bragg interference condition is then satisfied if $n_aL_a = n_bL_b$. The cavity is a $\lambda/2$-cavity characterised by a length L_c and a refractive index n_c, leading to a fundamental cavity resonance of angular frequency $\omega_c = \frac{\pi c}{n_cL_c}$. The structure is surrounded by vacuum with a refractive index $n_{\text{ext}} = 1$.

The central section of the cavity, of length L_x, is filled with an excitonic material characterised by the non-local susceptibility

$$\chi(z, z', \omega) = \sum_j \tilde{\chi}_j(\omega)\Phi_j^*(z)\Phi_j(z'), \tag{1}$$

where j indexes the normal-to-the-plane modes, with envelope functions $\Phi_j(z)$, z-direction is orthogonal to the planar system as shown in figure 1(c), z and z' are coordinates along z-axis.

$$\tilde{\chi}_j(\omega) = \frac{n_c^2\Omega_{\text{R}}^2\frac{\omega_x}{\omega_0}}{\omega_j^2 - \omega^2 - 2i\omega\gamma}, \tag{2}$$

is the local susceptibility. In equation (2) ω_j is the frequency of the jth optically active mode, γ the intrinsic matter losses, Ω_{R} the resonant vacuum Rabi frequency, proportional to the square root of the oscillator strength, and $\omega_x = \frac{2\pi c}{n_cL_x}$ is the frequency of a propagating electromagnetic mode with wavelength L_x. Note that in this formalism the factor $\omega_x \propto L_x^{-1}$ in the numerator of equation (2) assures that the value of Ω_{R} is an extensive property of the system, allowing us to perform a fair comparison between excitonic materials of different dimensionality, although the relation between Ω_{R} and the polariton splitting will involve a geometric factor of the order of 1.

For the QW case, see figure 1(a), we consider that modes beyond the lowest one (e.g. higher order excitons) are out of resonance and only retain the lowest ($j = 0$) optically-active mode, with frequency ω_0. Here, we introduce the reflection and transmission coefficients containing resonant excitonic contributions, to describe a QW. We consider the case where light is incident normally on a planar structure. We denote the amplitudes of incident, reflected and transmitted light as A_1^+, A_1^- and A_2^+, respectively. The reflection coefficient r is defined as the ratio of amplitudes of reflected light and incident light, $r = A_1^-/A_1^+$. The transmitted coefficient t is defined as the ratio of amplitudes of transmitted light and incident light, i.e. $t = A_2^+/A_1^+$. The QW layer is characterized by a reflection coefficient r_{QW} and transmission coefficient $t_{\text{QW}} = 1 + r_{\text{QW}}$. Following reference [18] they can be expressed in the form

$$r_{\text{QW}}(\omega) = \frac{\frac{i\omega}{2n_cc}\tilde{\chi}_0(\omega)\left[\int \Phi_0(z)\cos(kz)\text{d}z\right]^2}{1 - \frac{i\omega}{2n_cc}\tilde{\chi}_0(\omega)\left[\int \Phi_0(z)\cos(kz)\text{d}z\right]^2}, \tag{3}$$

with $\omega = \frac{ck}{n_c}$ and c the speed of light in vacuum. Assuming that the excitation profile is uniform across the layer of width $L_x \ll 1/k$ we then arrive at the expression for the amplitude reflection coefficient of the QW [28]

$$r_{\text{QW}} = \frac{i\pi\Omega_{\text{R}}^2}{\frac{\omega_0}{\omega}(\omega_0^2 - \omega^2) - 2i\omega_0\gamma - i\pi\Omega_{\text{R}}^2}. \tag{4}$$

Using different boundary conditions and excitation envelope functions would lead to analogous results (e.g. the Pekar boundary conditions would lead to a reduction of the vacuum Rabi frequency by a factor $\approx$0.9). Note that in order to be able to take into account arbitrary coupling strengths, we went beyond the usually employed single-pole approximation for the QW reflectivity [18] and used instead the full form of the susceptibility from equation (2).

In the bulk case, shown in figure 1(b), we consider instead the excitations to be dispersionless (that is $\omega_j = \omega_0\ \forall j$). This is usually a good approximation for bulk active resonances as optical phonons, bulk excitons, or organic microcavities, although the effect of dispersion can lead to observable non-local effects in sub-wavelength structures [29–31]. Neglecting the frequency dispersion of the exciton resonance and, as a consequence, neglecting the spatial dispersion in the cavity layer allows us to simplify the non-local

susceptibility exploiting the orthonormality condition $\sum_j \Phi_j^*(z)\Phi_j(z') = \delta(z-z')$, leading to a local polarization function

$$\mathbf{P}(\omega) = \epsilon_0 \tilde{\chi}_0(\omega)\mathbf{E}(\omega), \tag{5}$$

where $\mathbf{E}(\omega)$ is the local electric field. The local dielectric function can be derived from equation (5) and written as

$$\epsilon_B(\omega) = n_c^2 + \tilde{\chi}_0(\omega). \tag{6}$$

2.2. The transfer matrix model

In order to calculate the reflectivity of the full structures we apply the well-known transfer matrix method [18, 32] to study the reflectivity spectra and the complex frequencies of optical eigenmodes of the structure as functions of the vacuum Rabi frequency Ω_R. The transfer matrices of layers characterised by a frequency-independent dielectric function have a generic form

$$T_j = \begin{bmatrix} \cos(\omega n_j L_j/c) & i\,\sin(\omega n_j L_j/c)/n_j \\ i\,\sin(\omega n_j L_j/c) n_j & \cos(\omega n_j L_j/c) \end{bmatrix}, \tag{7}$$

with $j = \{a, b, c\}$ corresponding to the layers of Bragg mirrors and the cavity layer, respectively. For the bulk case we consider that the excitonic material completely fills the cavity ($L_c = L_x$) and we use as refractive index $\sqrt{\epsilon_B(\omega)}$, where the dispersive dielectric function has been defined in equation (6).

For the QW case we use instead the transfer matrix (denoted as T_{QW}) written in terms of its frequency-dependent reflection and transmission coefficients. In order to derive it, we suppose first that light is incident on a symmetric QW from the left side (right side), and the amplitude of electric field of the incident light is 1. Using Maxwell boundary condition for both sides of the QW embedded in a microcavity, [18] one will have

$$\begin{aligned} T_{\mathrm{QW}} \begin{pmatrix} 1 + r_{\mathrm{QW}} \\ n_c(1 - r_{\mathrm{QW}}) \end{pmatrix} &= \begin{pmatrix} t_{\mathrm{QW}} \\ n_c t_{\mathrm{QW}} \end{pmatrix}, \text{ for light from left side,} \\ \mathrm{T}_{\mathrm{QW}} \begin{pmatrix} t_{\mathrm{QW}} \\ -n_c t_{\mathrm{QW}} \end{pmatrix} &= \begin{pmatrix} 1 + r_{\mathrm{QW}} \\ -n_c(1 - r_{\mathrm{QW}}) \end{pmatrix}, \text{ for light from the right side,} \end{aligned} \tag{8}$$

where n_c is the refractive index while r_{QW} and t_{QW} are reflection and transmission coefficients of the background microcavity. Four equations in equation (8) describe the propagation of light incident from the left side and right side on a QW. Solving these equations one can obtain four elements of the transfer matrix as follows:

$$T_{\mathrm{QW}} = \frac{1}{2t_{\mathrm{QW}}} \cdot \begin{bmatrix} t_{\mathrm{QW}}^2 - r_{\mathrm{QW}}^2 + 1 & \dfrac{t_{\mathrm{QW}}^2 - (r_{\mathrm{QW}} + 1)^2}{n_c} \\ n_c(t_{\mathrm{QW}}^2 - (r_{\mathrm{QW}} - 1)^2) & t_{\mathrm{QW}}^2 - r_{\mathrm{QW}}^2 + 1 \end{bmatrix}. \tag{9}$$

For a QW, $t_{\mathrm{QW}} = 1 + r_{\mathrm{QW}}$ and equation (9) can be reduced to

$$T_{\mathrm{QW}} = \begin{bmatrix} 1 & 0 \\ 2n_c r_{\mathrm{QW}}/t_{\mathrm{QW}} & 1 \end{bmatrix}. \tag{10}$$

We denote the transfer matrix of the entire structure as T and its reflection coefficient as r. Expressing r through the elements of T, we obtain

$$r = \frac{n_{\mathrm{r}} t_{11} + n_{\mathrm{l}} n_{\mathrm{r}} t_{12} - t_{21} - n_{\mathrm{l}} t_{22}}{-n_{\mathrm{r}} t_{11} + n_{\mathrm{l}} n_{\mathrm{r}} t_{12} + t_{21} - n_{\mathrm{l}} t_{22}}, \tag{11}$$

where n_{r} and n_{l} are the refractive indices of right and left medium. In our case therefore $n_{\mathrm{r}} = n_{\mathrm{l}} = n_{\mathrm{ext}} = 1.0$. The reflectivity R can be now found as $R = |r|^2$. We shall focus on the optical eigenmodes of the structure that govern its optical response. One can find them imposing the boundary conditions of no light incident from right and left sides on the structure. In this case, one can represent the electric field of the light wave on the left side of the structure as $E_{\mathrm{l}} = \mathrm{e}^{-\mathrm{i}kz}$, and the magnetic field as $B_{\mathrm{l}} = -\frac{i}{ck_0}\partial_z E_{\mathrm{l}} = -\frac{k}{ck_0}\mathrm{e}^{-\mathrm{i}kz}$, where k is the wave vector of electromagnetic wave in the medium and k_0 is wave vector in vacuum. Since in our case the medium of environment is vacuum, $k = k_0$, therefore $cB_{\mathrm{l}} = -\mathrm{e}^{-\mathrm{i}kz}$. Further we chose the origin of the coordinate system such as $\mathrm{e}^{-\mathrm{i}kz} = 1$, that yields $E_{\mathrm{l}} = 1$ and $cB_{\mathrm{l}} = -1$. Similarly, the electromagnetic wave on the right side of the structure may be written in form $E_{\mathrm{r}} = A\mathrm{e}^{\mathrm{i}kz}$ and $cB_{\mathrm{r}} = Ae^{\mathrm{i}kz}$, where A is a complex coefficient. Absorbing complex $\mathrm{e}^{\mathrm{i}kz}$ in the coefficient A, electromagnetic wave on the right side can be written as $E_{\mathrm{r}} = A$ and $cB_{\mathrm{r}} = A$ At the normal incidence, the

solutions to the left- and right-hand sides of the structure are linked by the transfer matrix of the entire structure:

$$T\begin{pmatrix} E_{\rm l} \\ cB_{\rm l} \end{pmatrix} = \begin{pmatrix} E_{\rm r} \\ cB_{\rm r} \end{pmatrix} \Longrightarrow T\begin{pmatrix} 1 \\ -1 \end{pmatrix} = A\begin{pmatrix} 1 \\ 1 \end{pmatrix}. \tag{12}$$

Eliminating A, we derive the equation for complex eigenfrequencies

$$t_{11} - t_{12} - t_{21} + t_{22} = 0. \tag{13}$$

2.3. The second quantization model

Polaritons are best understood as hybrid quasiparticles, linear superposition of photonic and matter excitations. As such, Hamiltonian descriptions in terms of coupled discrete light and matter modes are a powerful tool to study their physics and phenomenology. Due to the interference-based reflectors considered in this work, and to the broad and extended nature of the Bragg modes outside of the stopband, an *ab initio* modal description would be nevertheless ill-suited.

In order to still develop an understanding of the transfer-matrix results for the QW case in terms of coupled oscillators, we model the system with a phenomenological Hamiltonian

$$H = \hbar\omega_0 b^\dagger b + \sum_n \hbar\omega_n a_n^\dagger a_n + \hbar\Omega_{\rm R}\sum_n f_n(a_n^\dagger + a_n)(b^\dagger + b), \tag{14}$$

describing a discrete matter resonance coupled to multiple discrete photonic modes. In equation (14), a_n and b are annihilation operators respectively for the nth photonic mode and an exciton, obeying the bosonic commutation relations

$$\left[a_n, a_m^\dagger\right] = \delta_{nm}, \quad \left[b, b^\dagger\right] = 1. \tag{15}$$

The overlap parameters f_n and the bare photonic frequencies ω_n can be used as fitting parameters. Such an Hamiltonian can be diagonalised by introducing the polaritonic annihilation operator

$$p = xb + zb^\dagger + \sum_n \left(y_n a_n + w_n a_n^\dagger\right), \tag{16}$$

where x, z, y_n and w_n are the complex Hopfield [33] coefficients obtained solving the eigenvalue equation

$$\omega p = \frac{1}{\hbar}\left[p, H\right]. \tag{17}$$

3. Numerical results and analysis

In the following, we investigate the reflectivity of symmetric model microcavity structures containing a QW or a bulk excitonic material. We vary the normalised coupling parameter $\eta = \Omega_{\rm R}/\omega_0$ to study how the system resonances shift and interact. In the simulations we used step sizes of 10^{-2} meV for energies and 10^{-4} for the normalised coupling η. The spatial resolution of structure geometry is 0.01 nm.

In an inorganic microcavity, tuning of the exciton oscillator strength may be achieved with use of external electric or magnetic fields, while in an organic cavity it can be done either by changing the molecular density [26] or by optically modifying the dipolar strength of the optically active transition [27]. For the sake of comparison, in both types of model structures we assume identical dielectric Bragg mirrors composed by eight periods, each consisting of the pair of dielectric layers aluminum nitride (AlN, layer a) and silicon nitride (SiN, layer b), with refractive indices $n_a = 2.02$ and $n_b = 1.96$ respectively.

In order to allow for an easy comparison between the results obtained in the QW and bulk cases, we used the same cavity parameters, with length $L_c = 134.0$ nm and $n_c = 1.75$. The lowest resonance of the $\lambda/2$ cavity is thus resonant with the optically active transition $\hbar\omega_0 = 2664.0$ meV. Note that in this configuration $\omega_x = 2\omega_0$. Detailed parameters for several organic microcavity candidates are listed in table 1.

3.1. Thin optical layer

The reflectivity spectrum of the symmetric microcavity structure with a QW embedded in its center is shown in figure 2(a). The QW intrinsic dissipation has been neglected ($\gamma = 0$) because of the long intrinsic exciton lifetimes in QWs and of the fact the radiative damping term (the $i\pi\Omega_{\rm R}^2$ in the denominator of equation (4)) is dominant in the regime of interest for us. Multiple interesting features are worth highlighting. Already in the stopband (from 2.59 to 2.70 eV), the two polaritonic resonances, whose splitting is usually proportional to the square root of η, strongly deviates from such a behavior. This

Table 1. Comparison of several organic microcavities.

Material	Exciton energy (eV)	Oscillator strength (cm^{-2})	η	ϵ
BODIPY [34]	2.66	1×10^{15}	0.05	1.75
4TBPPZn [23]	2.88	2×10^{15}	0.03	1.75
NTCDA [35]	2.70	—	0.06	1.6
Cyanine/PVA [36]	1.84	9×10^{14}	0.08	2.15
U3 [37]	1.57	—	0.02	—

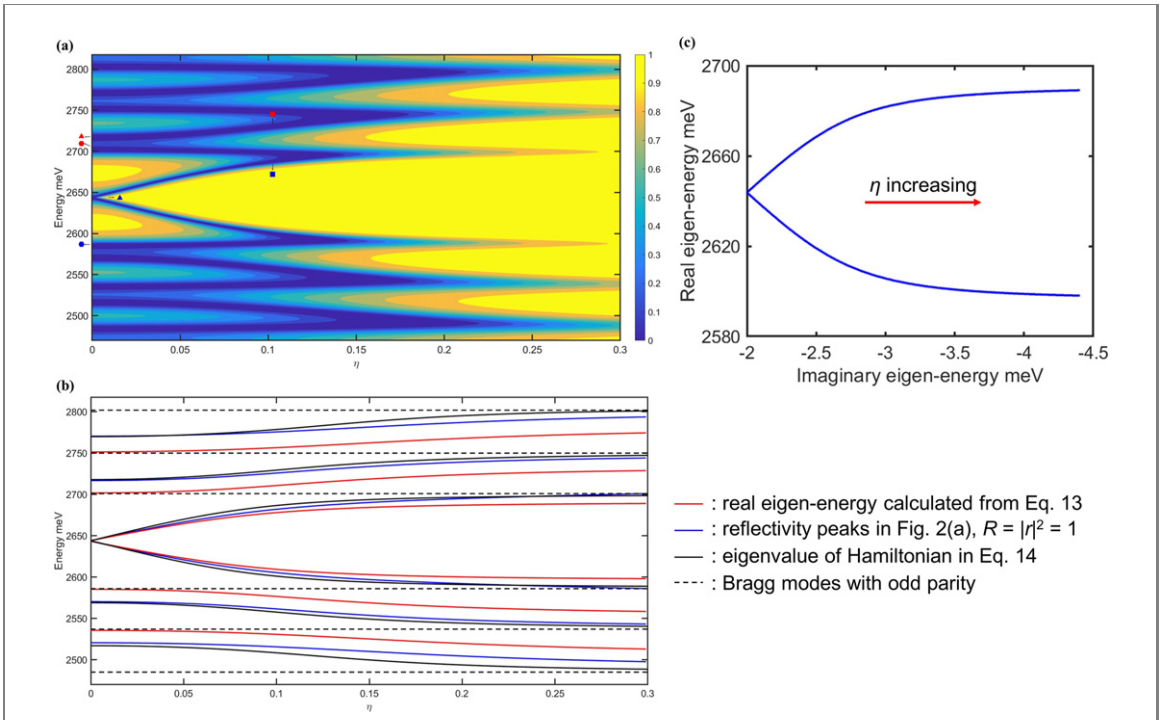

Figure 2. (a) Color plot of the reflectivity spectrum obtained using the transfer matrix method for a model symmetric microcavity structure with a QW embedded in its center as a function of the normalised coupling η. Hexagonal, triangle, and square symbols correspond to different electric field intensity curves in figure 3. (b) Photonic modes from reflectivity peaks (blue), eigenmode analysis (red), and Hamiltonian theory (black). Solid curves represent even Bragg modes, while dashed lines are modes with odd parity. (c) Eigenmode plot. The blue curve shows values taken by the complex eigen-energy of polariton modes as η increases. The increase of the imaginary part of the eigen-energy indicates the increase of radiative decay rate of polaritons due to their strong coupling with Bragg modes.

deviation can be documented already for relatively small values of the normalised coupling, saturating to the upper and lower edges of the main DBR stopband. Note the effective increase of the stop-band reflectivity and widening of the high reflectivity region with increase of the exciton–photon coupling strength that is apparent in figure 2(a). These effects are characteristic of the considered regime of interplay between the polariton Rabi-splitting and the Bragg stop-band width and linked with the optical metallization of dielectrics at large coupling strengths studied in reference [28]. In panel 2(c) we plot the real and imaginary part of the two polaritonic resonances in the stopband, varying the normalised coupling η. From such an image we can see that as the real polariton frequencies saturate, they also acquire an imaginary part, hybridising with the broad Bragg modes, which become a loss channel for the polariton energy.

Looking beyond the stopband in figure 2(a) we can see the emergence of a modal structure in which some modes are decoupled, and thus not influenced by the light–matter coupling η, while others do continuously and monotonously shifts from one decoupled photonic mode for $\eta = 0$ to the neighboring one for large η. This behavior of the shifting modes was already observed in the case of a 2D optically active layer coupled to multiple photonic modes. This phenomenon was explained as a consequence of the metallization of the optical response of the QW for large enough values of the coupling [28], but it can be also interpreted as a general consequence of the eigenmode structure of the linear light–matter coupling Hamiltonian [38].

This result strongly suggests the shifting resonances can be correctly identified as Bragg polaritons, resulting from the coupling of the QW exciton with the Bragg modes of the DBR. One unexplained feature remains in this picture, that is the presence of flat resonances, independent of η, within each the $\eta = 0$

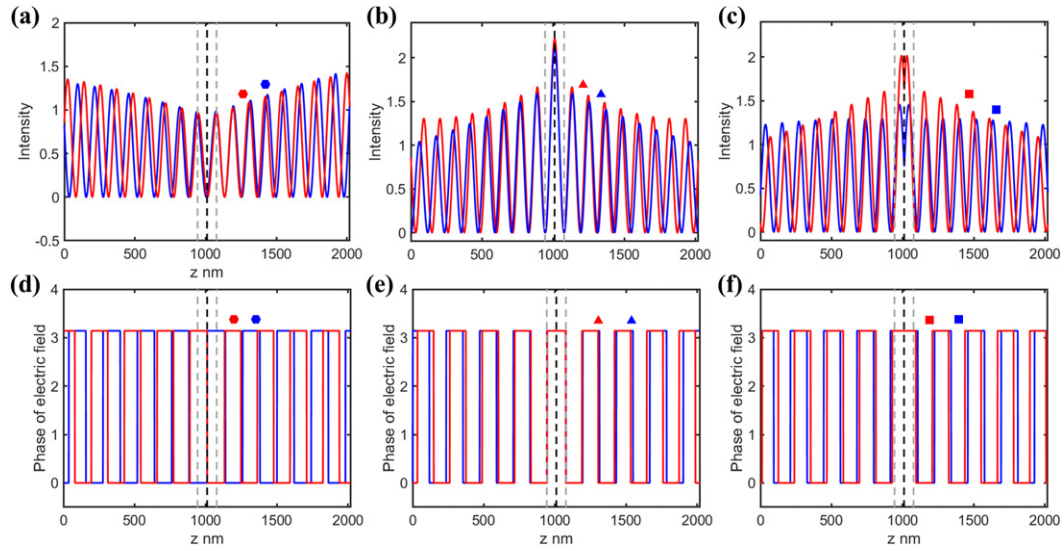

Figure 3. The electric field intensity profiles of the optical eigenmodes from figure 2(a), the black dashed line indicates the QW location, and the gray dashed lines indicate the interface of microcavity and Bragg mirrors. (a) The intensity of electric field ($I = |E|^2$, I is the intensity, E is the electric field) in the odd eigenmodes; (b) and (c) electric field distributions for even modes at $\eta = 0, \eta = 0.1$. (d), (e) and (f): phase of electric field corresponding to (a), (b) and (c) respectively.

Bragg modes. We interpret these uncoupled resonances as a peculiar feature of the photonic continuum, which can be more correctly described as an ensemble of narrow continuum bands [39]. Within each of these bands there are even and odd modes, the former coupled to the QW, the latter decoupled, as their electric field vanishes at the location of the QW in our symmetric structure. The modal structure is shown in figure 2(b), where we plot the peaks extracted from figure 2(a) (blue), and compare them with the ones obtained by the eigenmode analysis (red) and with a quasi-mode quantum theory fitted to the extracted peaks (black). We can see that the three models give qualitatively similar results, with even modes (solid) shifting and odd ones (dashed) uncoupled. The good agreement of such a simple model with the full transfer matrix calculation further supports our interpretation of each Bragg mode as a pair of broadened Fabry–Pérot modes having opposite parities. Note that the results obtained with the three approaches are not identical, and their difference increases moving further away from the stopband. This is expected because, as originally shown by Savona *et al* in reference [40], the results of a modal calculation and the reflectivity peaks do not coincide, and their difference increases with losses.

In order to validate our intuition on the origin of the coupled and uncoupled modes, in figure 3 we plot the photonic wavefunctions of the polaritonic resonances marked by respectively red and blue dots in figure 2(a). We can see how, consistently with our interpretation, the coupled Bragg modes are even while the decoupled ones are odd.

Note that Bragg polaritons have peculiar spatial extensions. In contrast to the cavity modes they penetrate far into the Bragg mirrors and couple to both surfaces of the structure. This greatly facilitates their coupling with external light modes, optical excitation and read-out. Moreover, hybrid Bragg modes in the strong coupling regime may be used to link vertically separated cavities in multiple-cavity structures that are currently discussed for applications as hyperbolic meta-materials [41] and double-qubit logic gates [42].

3.2. Bulk material

The reflectivity spectrum of a bulk organic microcavity system is presented in figure 4. The parameters of the model cavity have been chosen matching to those of the organic material 4,4-difluoro-4-bora-3a,4a-diaza-s-indacene (BODIPY) [34]. The linewidth of the excitonic material is taken $\gamma = 5$ meV [8]. Frenkel excitons in such material can be considered as infinitely heavy, thus providing a good model system. As the excitonic material is extended over half-wavelength of flight, parity selection rules are relaxed in bulk microcavities, so that excitons can couple with both even and odd optical modes in this case [43]. This spoils the parity-filtering effect seen in the QW case, where only even photon modes are able to couple with a QW exciton [44], and it leads to the appearance of a fan of higher-order polariton modes for $\omega < \omega_0$.

The absence of higher order modes for $\omega > \omega_0$, as well as the overall strong spectral asymmetry of figure 4, can be understood by noticing that the dielectric function in equation (6) is negative between the

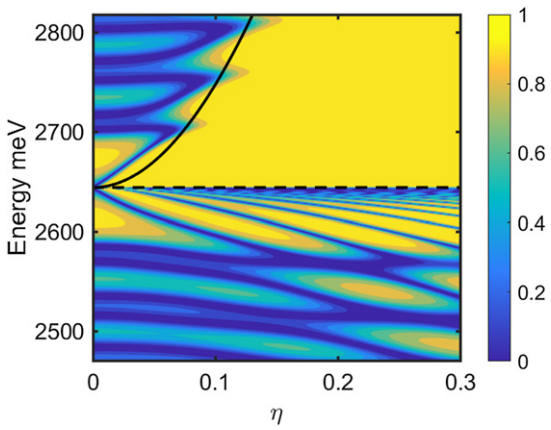

Figure 4. Color plot of the reflectivity spectrum obtained using the transfer matrix method for a model symmetric microcavity structure filled with a bulk optical material hosting excitons as a function of the normalised coupling η. The dashed black line represents the transverse frequency ω_{T} and the solid black line the longitudinal one ω_{L}. In the area between these two lines the excitonic material is highly reflective and microcavity effects vanish.

transverse (T) and longitudinal (L) frequencies

$$\omega_{\mathrm{T}} = \omega_0, \tag{18}$$

$$\omega_{\mathrm{L}} = \sqrt{\omega_0^2 + \Omega_{\mathrm{R}}^2 \frac{\omega_x}{\omega_0}}.$$

These frequencies are plotted in figure 4 with dashed and solid black lines, respectively. In such a frequency region, referred to as Reststrahlen band when the oscillator is an optical phonon, the excitonic material is strongly reflective. All cavity-induced effects thus disappear, because light cannot reach the second mirror.

These results demonstrate the existence of extended Bragg polaritons outside of the Reststrahlen band also in bulk materials. They also highlight a continuum transition between the strong coupling physics of organic molecules in a Bragg microcavity, and the optics of a single Bragg mirror over a highly conductive surface. The effective optical metallization of the organic semiconductor shown by our simulation, with the appearance of a broad Reststrahlen band in which the electromagnetic field cannot propagate, can be seen as the bulk equivalent of the decoupling effect predicted [28] and observed [45] in ultra-strongly coupled QWs.

4. Conclusions

We have examined theoretically a peculiar regime of light–matter coupling in a microcavity where the standard two-coupled oscillator model fails to capture the behavior of polariton and photon modes. This regime is achieved if the Rabi-splitting of polariton modes becomes comparable to the width of the stop-band of Bragg mirrors surrounding the cavity and offers an interesting and highly original phenomenology including the deviation of the Rabi-splitting from the predictions of a two-coupled oscillator model, the strong coupling of cavity polariton modes with Bragg modes of the corresponding parities, and the pronounced parity filtering effect of Bragg modes. The considered regime could become important for organic polariton lasers [46]. Our analysis has shown that this regime manifest itself as a continuous transition of the cavity polariton lasing mode into a Bragg polariton. Such a device would be characterised by a different mode volume and quality factor and, presumably, different threshold power and eventual topological properties. Our results thus broaden the parameter region of interest for recently developed organic polariton lasers. Further studies will investigate the specific lasing properties of the Bragg polaritons we described in this manuscript, and will investigate their technological usefulness. Furthermore, the considered light–matter coupling regime can be important for cavity-based frequency filters. We show that a cavity mode can be entirely removed from the stop band, which would enable one to switch on and off selective spectral filtering by acting upon excitons in microcavities with external electric fields. This effect could also find its applications in liquid crystal microcavities [47]. We expect that some of these phenomena may be observed in the reflectivity spectra of specially designed microcavities where the light–matter coupling strength may be tuned, e.g. with use of the photochemically induced conformational changes in organic molecules [27] or pumping an electron gas in the excitonic material [48]. These results

open the new path for band engineering in photonic structures. They have a significant fundamental interest as they shed light on the light–matter coupling beyond the two-coupled oscillator model.

Acknowledgments

AK and JC are supported by Westlake University, Project 041020100118 and Program 2018R01002 funded by Leading Innovative and Entrepreneur Team Introduction Program of Zhejiang Province of China. SDL is a Royal Society Research Fellow and was partly funded by the Philip Leverhulme Prize of the Leverhulme Trust and the RGF\EA\181001 Grant of the Royal Society.

Data availability statement

All data that support the findings of this study are included within the article (and any supplementary files).

ORCID iDs

Junhui Cao https://orcid.org/0000-0003-1101-9287

References

[1] Weisbuch C, Nishioka M, Ishikawa A and Arakawa Y 1992 Observation of the coupled exciton–photon mode splitting in a semiconductor quantum microcavity *Phys. Rev. Lett.* **69** 3314
[2] Schneider C *et al* 2013 An electrically pumped polariton laser *Nature* **497** 348–52
[3] Laussy F P, Kavokin A V and Shelykh I A 2010 Exciton–polariton mediated superconductivity *Phys. Rev. Lett.* **104** 106402
[4] Berloff N G, Silva M, Kalinin K, Askitopoulos A, Töpfer J D, Cilibrizzi P, Langbein W and Lagoudakis P G 2017 Realizing the classical *XY* Hamiltonian in polariton simulators *Nat. Mater.* **16** 1120
[5] Cuevas A *et al* 2018 First observation of the quantized exciton–polariton field and effect of interactions on a single polariton *Sci. Adv.* **4** eaao6814
[6] Ballarini D, De Giorgi M, Cancellieri E, Houdré R, Giacobino E, Cingolani R, Bramati A, Gigli G and Sanvitto D 2013 All-optical polariton transistor *Nat. Commun.* **4** 1778
[7] Ballarini D *et al* 2020 Polaritonic neuromorphic computing outperforms linear classifiers *Nano Lett.* **20** 3506–12
[8] Ballarini D and De Liberato S 2019 Polaritonics: from microcavities to sub-wavelength confinement *Nanophotonics* **8** 641–54
[9] Frisk Kockum A, Miranowicz A, De Liberato S, Savasta S and Nori F 2019 Ultrastrong coupling between light and matter *Nat. Rev. Phys.* **1** 19–40
[10] Forn-Díaz P, Lamata L, Rico E, Kono J and Solano E 2019 Ultrastrong coupling regimes of light–matter interaction *Rev. Mod. Phys.* **91** 025005
[11] Khurgin J B 2001 Excitonic radius in the cavity polariton in the regime of very strong coupling *Solid State Commun.* **117** 307–10
[12] Brodbeck S, De Liberato S, Amthor M, Klaas M, Kamp M, Worschech L, Schneider C and Höfling S 2017 Experimental verification of the very strong coupling regime in a GaAs quantum well microcavity *Phys. Rev. Lett.* **119** 027401
[13] Ruggenthaler M, Tancogne-Dejean N, Flick J, Appel H and Rubio A 2018 From a quantum-electrodynamical light–matter description to novel spectroscopies *Nat. Rev. Chem.* **2** 0118
[14] Averkiev N S and Glazov M M 2007 Light–matter interaction in doped microcavities *Phys. Rev.* B **76** 045320
[15] Levinsen J, Li G and Parish M M 2019 Microscopic description of exciton–polaritons in microcavities *Phys. Rev. Res.* **1** 033120
[16] Cortese E, Carusotto I, Colombelli R and De Liberato S 2019 Strong coupling of ionizing transitions *Optica* **6** 354–61
[17] Cortese E, Tran N-L, Manceau J-M, Bousseksou A, Carusotto I, Biasiol G, Colombelli R and De Liberato S 2021 Excitons bound by photon exchange *Nat. Phys.* **17** 31–5
[18] Kavokin A (ed) 2007 *Microcavities: 16* (*Series on Semiconductor Science and Technology*) (Oxford: Oxford University Press) OCLC: ocn153553936
[19] Zhang Q, Lou M, Li X, Reno J L, Pan W, Watson J D, Manfra M J and Kono J 2016 Collective non-perturbative coupling of 2D electrons with high-quality-factor terahertz cavity photons *Nat. Phys.* **12** 1005
[20] De Liberato S 2015 Perspectives for gapped bilayer graphene polaritonics *Phys. Rev.* B **92** 125433
[21] Low T *et al* 2017 Polaritons in layered two-dimensional materials *Nat. Mater.* **16** 182–94
[22] Rupprecht C, Lundt N, Wurdack M, Stepanov P, Estrecho E, Richard M, Ostrovskaya E A, Höfling S and Schneider C 2021 Micro-mechanical assembly and characterization of high-quality Fabry–Pérot microcavities for the integration of two-dimensional materials *Appl. Phys. Lett.* **118** 103103
[23] Lidzey D G, Bradley D D C, Skolnick M S, Virgili T, Walker S and Whittaker D M 1998 Strong exciton–photon coupling in an organic semiconductor microcavity *Nature* **395** 53–5
[24] Liu X, Galfsky T, Sun Z, Xia F, Lin E-c, Lee Y-H, Kéna-Cohen S and Menon V M 2015 Strong light–matter coupling in two-dimensional atomic crystals *Nat. Photon.* **9** 30
[25] Gubbin C R, Maier S A and Kéna-Cohen S 2014 Low-voltage polariton electroluminescence from an ultrastrongly coupled organic light-emitting diode *Appl. Phys. Lett.* **104** 233302
[26] Gambino S *et al* 2014 Exploring light–matter interaction phenomena under ultrastrong coupling regime *ACS Photon.* **1** 1042
[27] Schwartz T, Hutchison J A, Genet C and Ebbesen T W 2011 Reversible switching of ultrastrong light–molecule coupling *Phys. Rev. Lett.* **106** 196405
[28] De Liberato S 2014 Light–matter decoupling in the deep strong coupling regime: the breakdown of the Purcell effect *Phys. Rev. Lett.* **112** 016401

[29] Quattropani A, Andreani L C and Bassani F 1986 Quantum theory of polaritons with spatial dispersion: exact solutions *Nuovo Cim.* D **7** 55–69
[30] Gubbin C R and De Liberato S 2020 Optical nonlocality in polar dielectrics *Phys. Rev.* X **10** 021027
[31] Rajabali S, Cortese E, Beck M, De Liberato S, Faist J and Scalari G 2021 Polaritonic Nonlocality in light–matter interaction *Nat. Photon.* **15** 690–5
[32] Gubbin C R and De Liberato S Dec 2020 Nonlocal scattering matrix description of anisotropic polar heterostructures *Phys. Rev.* B **102** 235301
[33] Hopfield J J 1958 Theory of the contribution of excitons to the complex dielectric constant of crystals *Phys. Rev.* **112** 1555
[34] Yagafarov T *et al* 2020 Mechanisms of blueshifts in organic polariton condensates *Commun. Phys.* **3** 18
[35] Holmes R J and Forrest S R 2004 Strong exciton–photon coupling and exciton hybridization in a thermally evaporated polycrystalline film of an organic small molecule *Phys. Rev. Lett.* **93** 186404
[36] Hobson P A, Barnes W L, Lidzey D G, Gehring G A and Walker S 2002 Strong exciton–photon coupling in a low-q all-metal mirror microcavity *Appl. Phys. Lett.* **81** 3519–21
[37] Wenus J, Ceccarelli S, Lidzey D G, Tolmachev A I, Slominskii J L and Bricks J L 2007 Optical strong coupling in microcavities containing j-aggregates absorbing in near-infrared spectral range *Org. Electron.* **8** 120–6
[38] Todorov Y 2014 Dipolar quantum electrodynamics theory of the three-dimensional electron gas *Phys. Rev.* B **89** 075115
[39] Gerace D and Andreani L C 2005 Strong exciton–light coupling in photonic crystal nanocavities *Phys. Status Solidi (c)* **2** 801–4
[40] Savona V, Andreani L C, Schwendimann P and Quattropani A 1995 Quantum well excitons in semiconductor microcavities: unified treatment of weak and strong coupling regimes *Solid State Commun.* **93** 733–9
[41] Sedov E S, Iorsh I V, Arakelian S M, Alodjants A P and Kavokin A 2015 Hyperbolic metamaterials with Bragg polaritons *Phys. Rev. Lett.* **114** 237402
[42] Xue Y, Chestnov I, Sedov E, Schumacher S, Ma X and Kavokin A 2021 Split-ring polariton condensates as macroscopic two-level quantum systems *Phys. Rev. Res.* **3** 013099
[43] Chen Y, Tredicucci A and Bassani F 1995 Bulk exciton polaritons in GaAs microcavities *Phys. Rev.* B **52** 1800
[44] Tredicucci A, Chen Y, Pellegrini V, Börger M and Bassani F 1996 Optical bistability of semiconductor microcavities in the strong-coupling regime *Phys. Rev.* A **54** 3493–8
[45] Bayer A, Pozimski M, Schambeck S, Schuh D, Huber R, Bougeard D and Lange C 2017 Terahertz light–matter interaction beyond unity coupling strength *Nano Lett.* **17** 6340
[46] Dusel M, Betzold S, Harder T H, Emmerling M and Klembt S 2021 Room-temperature topological polariton laser in an organic lattice *Nano Lett.* **21** 6398–405
[47] Lekenta K *et al* 2018 Tunable optical spin hall effect in a liquid crystal microcavity *Light: Sci. Appl.* **7** 74
[48] Günter G *et al* 2009 Sub-cycle switch-on of ultrastrong light–matter interaction *Nature* **458** 178